Damage detection for laminated composites using full-field digital image correlation

C.J Qambela[1], P.S Heyns[2], H.M Inglis[3]
Centre for Asset Integrity Management
University of Pretoria
Pretoria
u29303479@tuks.co.za

ABSTRACT

Laminated composites are complex multifunctional materials and often endure barely visible damage which is characterised by matrix cracks and fiber damage leading to delamination. These composites are often used in safety-critical industries such as aeronautical and automotive industries which makes it crucial to have techniques to assess damage before and during use. This paper presents full-field digital image correlation (DIC) as a method for damage detection in laminated composites under static loading conditions. Full-field digital image correlation is an optical measuring system used to assess deformation data (i.e. displacement and strain) in any component under various loading conditions. Assuming that the damage changes the mechanical properties, the method is applied here to detect changes in stiffness caused by barely visible impact damage (BVID) in laminated composites.

It is shown in the experimental findings that full-field digital image correlation has the capability to detect barely visible damage caused by various impact energies in laminated composites, provided that the excitation or form of loading is applied near the impacted area.

KEYWORDS: full-field DIC, laminated composite, BVID

1. INTRODUCTION

A composite is any material that comprises of two or more constituents bounded together to function as a single component. Laminated composites consist of two major components i.e. the matrix and the reinforcements. The matrix in most cases is formed from epoxy resin and functions as the adhesive in the laminated composites. The reinforcements are the fibers of materials such as carbon or glass held together by the matrix and are responsible for most of the strength of the material [1].

Laminated composites can be produced by hand layup or automatic fiber placement. When the composite is manufactured by hand the fibers are laid up in the desired orientation and liquid resin is added to surround the fibers and spaces between them. The mixture is then left to cure and harden forming the composite. Laminated composite manufacturing by automatic fiber placement uses

fabrics which have been pre-impregnated with resin known as prepreg fabrics or plies, application of heat and pressure bind the fabrics together.

Laminated composites have become increasingly popular due to their high strength-to-weight [2] and stiffness-to-weight ratios [3] for lightweight construction in the aerospace and aeronautical industries. Unlike isometric material such as steel and aluminium, composites are weak to impact damage and the resulting damage mechanisms such as matrix cracks, fiber breakage and delamination are difficult to detect by visual inspection. The layered structure of laminated composites makes it difficult to detect barely visible impact damage which may lead to critical material failure. For safe and reliable use of laminated composites throughout the design life, non-destructive testing (NDT) has become one of the most crucial aspects of successful application of composite materials. Since this research aims to demonstrate full-field DIC as a capable NDT method, similar existing methods are discussed along with their limitations and attributes.

There are various NDT techniques applicable for damage detection in laminated composites depending on how the stimuli interacts with nature of the damage. Delamination for instance results in air pockets becoming entrapped within the composites. With the use of radiography the delamination can be detected [4] including any fiber wrinkles and non-uniform fiber distributions. Damage in laminated composites tends to also alter the thermal conductivity of the material. Thermography takes advantage of the changes in these properties throughout the material to highlight defects [4]. However, the technique of thermography is limited to thin composites as any defects that lie deeper under the surface of the material tend to create less heat fluctuation for adequate detection. It has been demonstrated that thermography can detect smaller impact damage sizes more effectively than radiography in laminated composites of varying ply layups [5-6].

Ultrasonic testing is one of the most commonly used NDT methods suitable for damage detection, the method uses high frequency sound waves to detect defects such as porosity, translaminar cracks and foreign inclusions [7]. Pulse-echo ultrasonic testing has been shown to be effective in detecting inconsistencies in homogenous materials. Through-transmission ultrasonic testing is more useful for damage detection in parts with complex geometries [7]. Ultrasonic C-scan has been demonstrated as the best performing method for damage detection of various forms such as hole and impact damage in laminated composites as opposed to the method thermography [8]. From ultrasonic C-scan images parameters of the defect such as size and depth can be obtained.

Another effective NDT method for laminated composites is acoustic emission. It differs from the methods discussed thus far in that instead of supplying energy to the part and measuring the returning signals, the method listens to sound generated by energy released in the object. Imperfections such as matrix cracks and fiber breakage result in stress waves which can be detected by highly sensitive piezo-electronics.

Studies [9-10] have been conducted on using modal analysis to detect damage in laminated composites. It has been found that shifts in the values of the natural frequencies on the frequency response function occur as a result of damage. The shifts in the natural frequencies become more noticeable in the high frequency range. Modal analysis is useful in that damage tends to causes changes in the stiffness (and to a lesser extent mass) of a component which in turn alters the vibrational characteristics of the material.

Since composite materials exhibit damage in a complex manner, various data processing methods have also been investigated for the purpose of damage inspection, based on present methods. One dimensional Fourier transforms and wavelets have been used for thermographic data processing have proved accurate in detecting matrix cracks and delamination under thermal excitation [11]. Improvements on continuous and discrete wavelet transformations by signals derived from low and high frequency modes proved effective in detecting matrix damage [12] in numerical models of laminated composites. Damage can also cause changes in the electrical responses of components. Lamb waves have been used effectively for damage detection in which the composites has suffered loss of mass such as hole damage [13]. The incorporation of wavelet transform for signal processing in Lamb wave excitation has been shown to improve detection of microstructural damage [14].

All NDT techniques function on the basis that damage causes changes in the properties of the component such as stiffness, mass, thermal properties and electrical properties. Almost all have lengthy procedures that need to be followed for accurate detection and are applicable to components of certain sizes and geometry. The work on full-field DIC presented in this paper shows that DIC can be applied as a damage detection method for laminated composites. The method has the benefit of non-contact between the subject and the instrumentation, the force needs to be physically applied to specimens near the damage area in order to detect the damage and strain data is not very sensitive. The method is useful when one is interested in detecting the change in stiffness as a result of the damage at a known location on the composite.

2. FULL-FIELD DIC

DIC is a non-contact optical measuring system that functions on the principles of photogrammetry, stereo imaging and image processing to record material deformations during loading [15-16]. The system defines displacement and strain fields by applying the deformation theory of solid mechanics. Displacement can be defined as the change in position from a reference point or location, while strain is derived from displacement data and is the ratio of a material change in dimension from external loading to its original dimension [17]. DIC makes use of high speed cameras to record the deformation of the test subject as it is being loaded. The surface of the test subject is prepared prior to the experiment by introducing scattered black speckles on a white background. Each speckle on the subject surface is tracked from the first image that is captured to the last one in the series. From the

change in speckle location due to the loading, displacement and strain fields are computed by the DIC data acquisition system. Full-field DIC involves the use of multiple cameras placed to face the test subject at different angles in order to produce three-dimensional results (i.e. x, y and z components of displacement and strain).

3. DESCRIPTION OF LAMINATED COMPOSITE SPECIMENS

For the experiments, three 300 mm × 300 mm × 1mm fully fabricated carbon/epoxy woven laminated plates were purchased. The first two plates were labeled plate A, plate B. From each plate, four pieces of the required dimensions (i.e. 156 mm × 133 mm × 1 mm) were cut out using an electric band saw. Plate A1′ and B3′ in Figure 1 were cut from the third plate to replace the specimens which were damaged during preparation. Four 10.3 mm holes were drilled on each specimen as fixture locations using M10 bolts for the experimental setup for impact tests and full-field DIC under static loading.

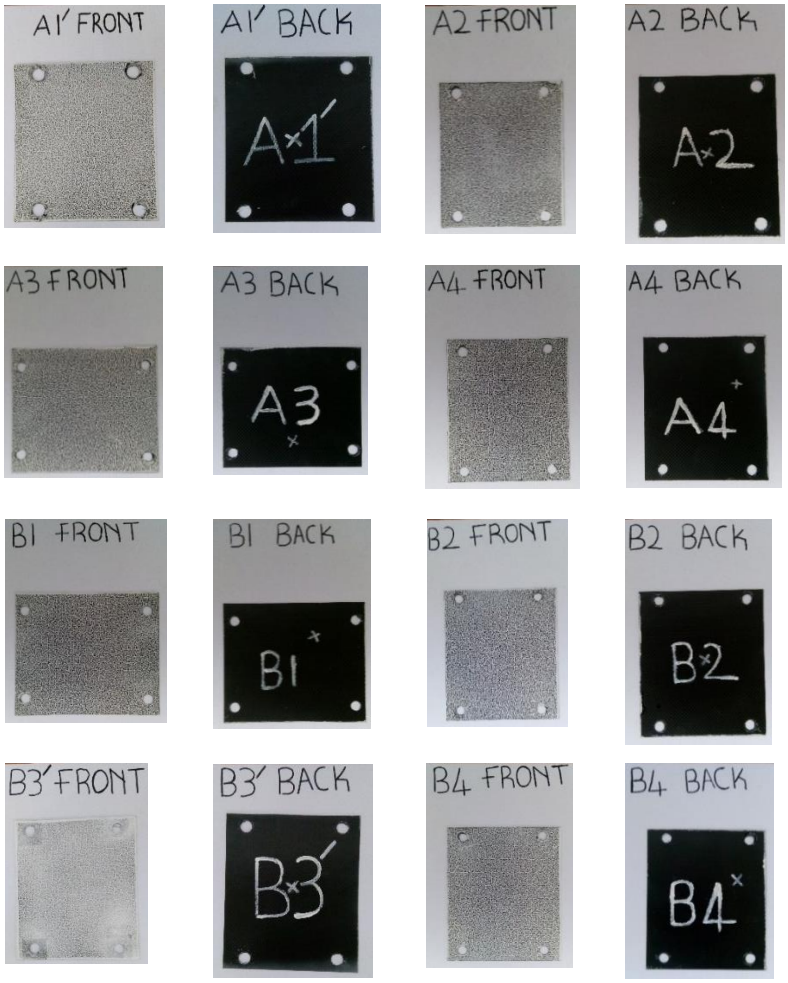

Figure 1: Carbon/epoxy woven laminated specimens showing the front and back face of each specimen after the final step of surface preparation

The specimens were given 3 coats of matt white spray paint as part of surface preparation. When dry the scattered dot stencils were applied on the white surfaces as the final step of surface preparation for full-field DIC.

The back face of each laminate was labeled according to the plates they were cut from, and the locations for centered and off-centered impact were marked with a cross using a permanent white marker as shown in Figure 1.

4. EXPERIMENTAL SETUP

Two experimental setups were used in the investigation, a drop impact apparatus for inducing barely visible damage on the laminated composite specimens at various impact energies. Carbon/epoxy woven laminated composites were subjected to static loading conditions before and after the impact, with the application of a point load. Their deformation data (i.e. out-of-plane displacement and von Mises strain fields) was captured using full-field DIC prior and post the impact in order to compare changes in deformation data as a result of the induced damage.

The investigation was structured to evaluate at what impact energy the induced barely visible impact damage becomes detectable using full-field DIC under static loading conditions. To eliminate any bias in the experimentation the specimens cut from plate A and B were mixed for the centered and off-center impact as shown in table 1.

Table 1: Assignment of specimens for the centered and off-centered impact energies

Impact energy	Centered impact	Off- centered impact
3 J	Specimen A1′	Specimen B1
6 J	Specimen B3′	Specimen A4
9 J	Specimen A2	Specimen B4
12 J	Specimen B2	Specimen A3

To account for the variability introduced in the measurements by full-field DIC under static loading conditions and the experimental setup, repeated experiments on one of the specimens (i.e. Specimen B2) were conducted and are presented first in the results. The repeated experiments included recalibration of the cameras and dismantling of the specimen after some tests prior and post the impact.

Barely visible impact damage can be caused by various impact energies depending on the thickness of the composite. 1 mm thick laminated composites were subjected to varying impact energies of 3 J, 6 J, 9 J, and 12 J in order to study at what energy level the damage becomes detectable using full-field DIC under static loading conditions. Based on literature looking into load vs displacement behaviour for different laminates of different thickness [18], it was not expected that 3 J of impact energy to result in detectable damage.

4.1 Drop impact test experimental setup

Figure 2 shows the schematic representation of the constructed drop impact apparatus that was used to induce barely visible impact damage in the laminated composite specimens. Figure 3 shows the actual apparatus for the drop tests, two 12 mm steel rods were used to construct a guide frame for the sliding impactor. A 1.4 kg mass with a rounded end was used as the impactor. Two 18 mm holes were drilled on the weight attached to the impactor to enable it to slide smoothly from the required height as shown in Figure 3(b). A 400 mm × 400 mm × 15 mm steel base plate with a 100 mm x 110 mm cut-out was used to support the specimens using M10 bolts from the bottom face of the plates. The cut-out exposed enough of the area of the back faces of the laminated composite specimens for centered and off-centered impacts. The steel base plate could be moved so as to align the marked points on the specimen with the tip of the impactor. The heights of the impactor for the required impact energies were marked on the guide rods. For each test, the impactor was simply raised to the required height and allowed to drop down to the specimen.

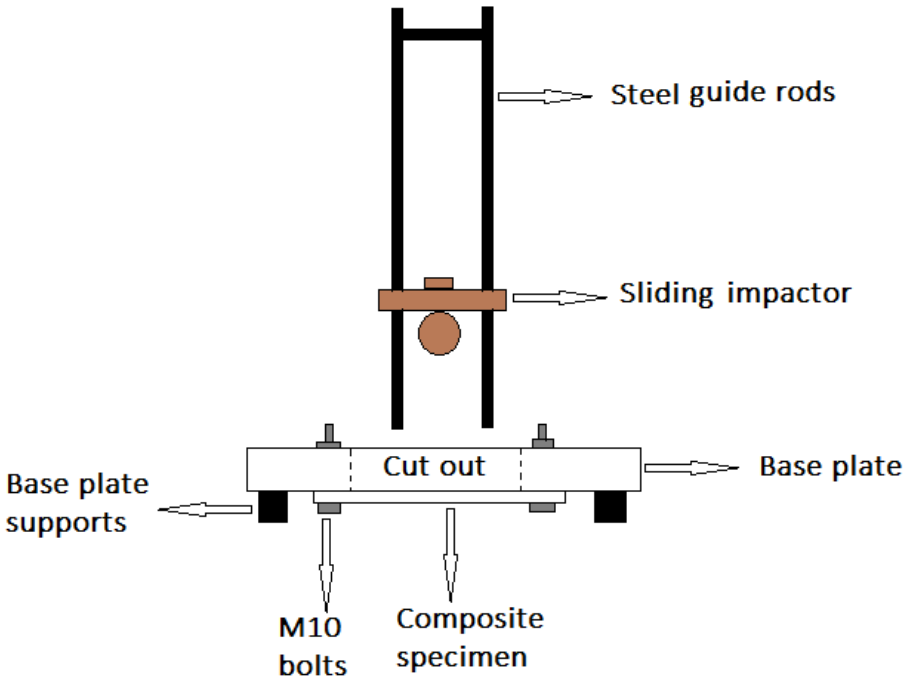

Figure 2: Simplified schematic representation of the drop impact apparatus

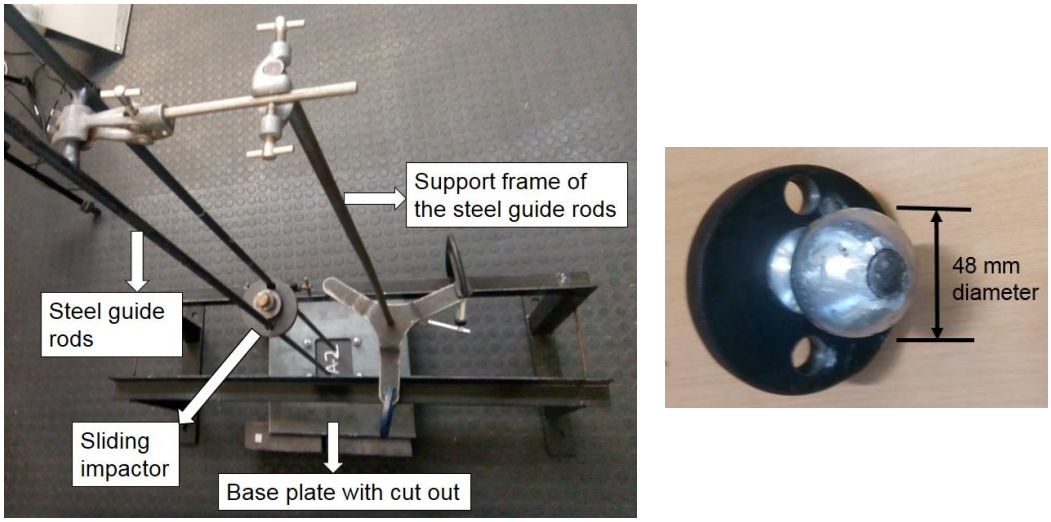

(a) (b)

Figure 3: Actual drop test apparatus: (a) shows the setup, (b) shows the 1.4 kg impactor

4.2 Full-field DIC experimental setup

Figure 4 shows a simplified schematic representation of the actual full-field DIC experimental setup (Figure 5) that was used for damage detection in laminated composites under static loading conditions. A holding plate was used to secure the specimens using M10 bolts (Figure 5(c)). The holding plate itself was attached to the test frame of the setup using M10 bolts. The front of the test frame has a cut out which exposes an area of 220 mm × 110 mm of the laminated composites to the full-field DIC cameras as shown in Figure 5(b). A pneumatic actuator was used to exert the forces on the back face of the laminated composites via a 24 mm steel piston with a rounded tip which slid through the hole on the holding plate.

A calibrated 200 kg load cell was used to measure the forces applied to the specimens. The load cell was connected to the DIC data acquisition system as an external trigger. The Images were captured according to the set trigger list of loads in voltage form.

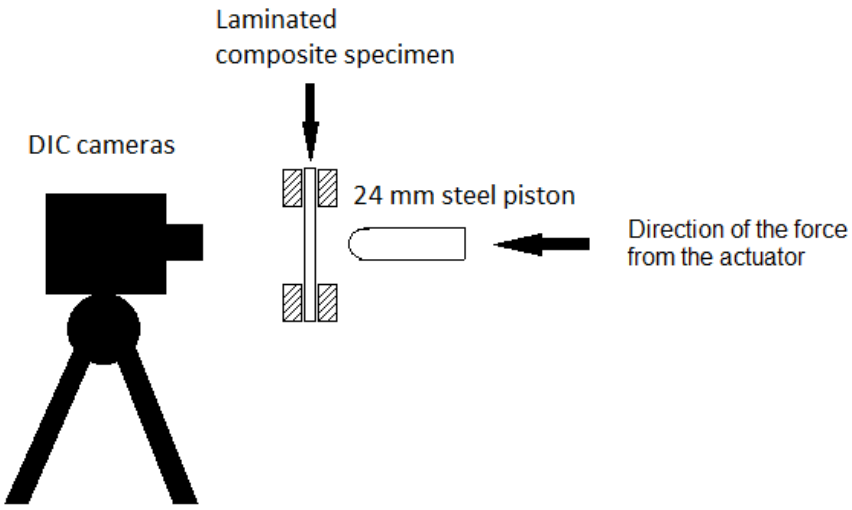

Figure 4: Simplified schematic representation of full-field DIC setup for damage detection under static loading

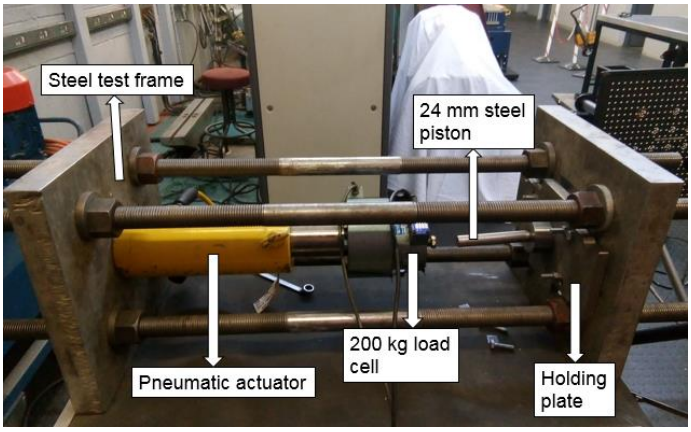

(a)

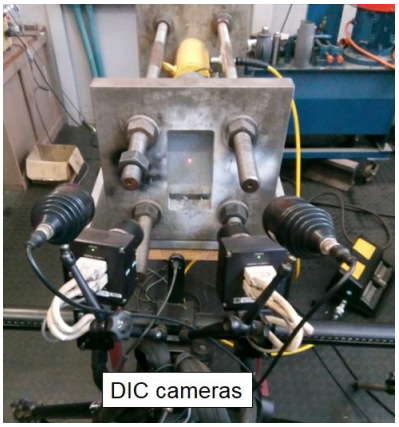

(b)

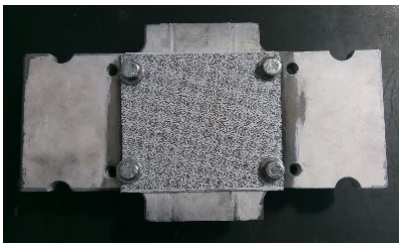

(c)

Figure 5: Experimental setup for the full-field DIC: (a) shows the side view of the setup, (b) shows the front view with the DIC cameras, (c) shows the holding plate with specimen attached to it using M10 bolts

Figure 6 shows the camera setup for calibration process of the full-field DIC GOM cameras. The cameras were mounted on a slider which is equipped with a laser to aid with centering of the cameras. Once the adjustments of the lenses and lights rendered images with sufficient contrast the cameras were calibrated using a calibration panel Figure 6(a).

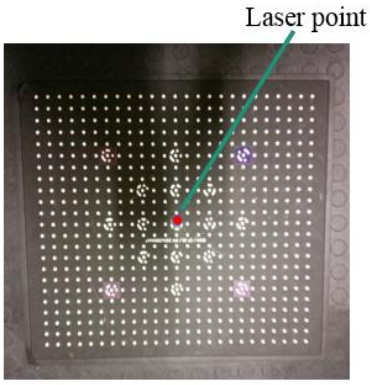

(a) Calibration panel with 17 main points

(b) Camera calibration setup

Figure 6: Full-field DIC calibration setup: (a) shows the calibration panel, (b) shows camera and calibration panel setup

The panel was magnetically supported on its own tripod which had to be placed a measuring distance 480 mm away from the cameras for calibration. A calibration distance of less or more than the measuring distance of 480 mm would lead to inaccurate measurements.

The panel was positioned such that the vertical cross hairs intersected with the laser point in the image observed on the left and right camera.

Calibration was carried out with instructions using the Aramis GOM software and it is necessary in order to determine the distance and orientation of the cameras to each other, as well as the image characteristics of the lenses. Based on the settings such as lens distortion and focus, the software calculates the three-dimensional coordinates from the reference point of the calibration panel in the two-dimensional camera image. Multiple images of the calibration panel were taken at different angles and positions with all 17 main points on the panel captured by both cameras. Should some of the main points on the panel be visible in the captured image of one of the cameras and not on the other a high calibration deviation value in the calibration results would be obtained. The calibration deviation is computed from the average reference point deviation of all main dots recorded during the process of calibration and should be between 0.01 and 0.07 pixels [19]. A calibration deviation value larger than 0.07 would lead to incorrect scale parameters, a calibration deviation range of 0.047 and 0.066 was obtained in the experiments.

5 EXPERIMENTAL RESULTS

5.1 Variations in full-field DIC measurements

Figure 7 shows the results of specimen B2 which was subjected to 12 J of centered impact energy. The specimen was also used to establish variations in full-field DIC measurements introduced by recalibrating of the cameras and repeated tests including dismantling of the specimen.

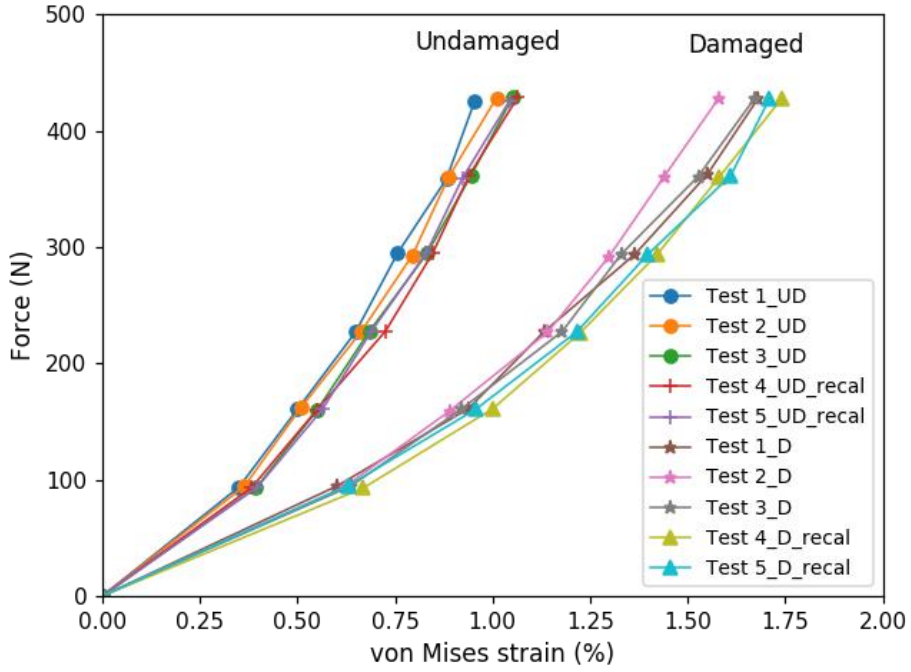

Figure 7: Full-field DIC von Mises strain measurements of specimen B2 repeated test and camera recalibration before and after the impact of 12 J, where “UD” stands for undamaged, “D” stands for damaged and “recal” stands for recalibration of the cameras

Figure 7 shows the force vs von Mises strain curves of specimen B2 before and after the centered impact of 12 J. On the legend of the plot “UD” stands for undamaged and “D” stands for damaged and “recal” stands for recalibration of the cameras.

The von Mises strain data is one of the outputs of the full-field DIC system. The strain data of each image during deformation was extracted and plotted using python. The specimen was subjected to six loads as defined in the trigger list. The curves of the undamaged B2 specimen show that a variation exists between repeated test without dismantling and recalibrating the cameras between tests (test 1-3). Test 4 and 5 include dismantling of the specimens and recalibration of the cameras between the tests. No significant variation exists between the tests as the curves of some of the tests with and without recalibration of the cameras sometimes coincide. The small variation between the tests may be a result of slight voltage fluctuations from the load cell resulting in exact or slightly higher or lower loads than stated in the trigger list. An immediate noticeable difference in Figure 7 lies in the increase in strain values after the impact. The barely visible damage caused by an impact of 12 J resulted in a more compliant specimen (degraded stiffness). The difference in strain values between the undamaged and damaged B2 specimen increased with increasing load. Regardless of the variation in measurements a clear distinction in stiffness due to the impact is evident from the curves.

Table 2 summarizes the range in variation observed from von Mises strains measurements obtained between the tests for specimen B2. From table 2 it can be concluded that a maximum variation in von Mises strain of about 0.2% is observed between repeated tests.

Table 2: Variation range percentage von Mises strains between repeated tests including dismantling and camera recalibration

	Undamaged B2 specimen	Damaged B2 specimen
Variation range	0 - 0.1 %	0 - 0.16 %

Figure 8 shows the von Mises strain fields for the load of 295 N of three tests (test 1 - 3) which were done without dismantling specimen B2 which was subjected to 12 J of centered impact energy. The strain field is in agreement in terms of the shapes. Of particular interest in Figure 8 is that the peak strains occur at different locations in the three tests where the point loads were applied. This demonstrates that so long as the load is applied near the impacted area (i.e. the center in this case) the loss in stiffness due to barely visible impact damage can be detected.

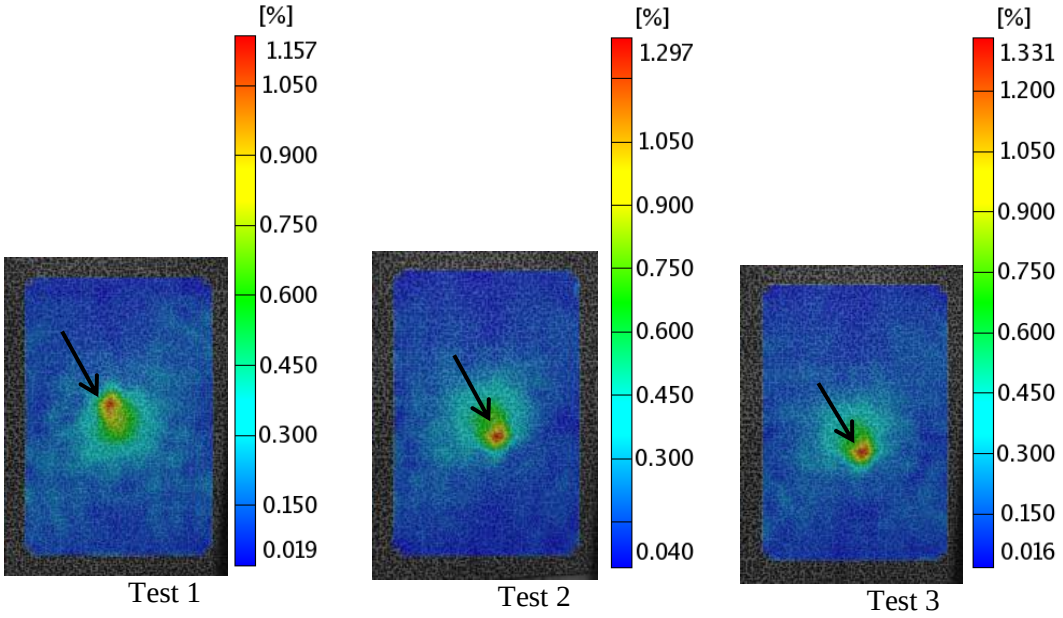

Figure 8: von Mises strain fields of three test of specimen B2 after 12 J of impact showing the load of 295 N applied at different locations near the impacted area

5.2 Full-field DIC results of specimens subjected to centered impact

Figure 9(a) shows the full-field DIC results for first specimen (A1′) which was subjected to a centered impact energy of 3 J. Figure 9(a) shows the force vs out-of-plane displacement curves and the force vs von Mises strain curves before and after the impact. Three tests were conducted for repeatability in each case. Both the out-of-plane displacements and von Mises curves show no change in stiffness due to the impact of 3 J, on all curves the values of the out-of-plane displacements and von Mises strains coincide for every test conducted before and after the impact with increasing load. The results suggest that the impact energy of 3 J did not cause any significant damage detectable by using full-field DIC, or the impact energy was too low to cause any damage. The specimen showed very little deformation after the impact as shown in Figure 9(b), the cross on the specimen marks the location of the impact. The deformation however was not permanent, the specimen reverted to its original form once it was unbolted from the base plate of the drop impact apparatus. The impact energy of 3 J resulted in no damage as demonstrated by the full-field DIC results of specimen A1′, this suggests that the 1 mm thick laminates are resistant to that amount of impact energy as expected [18].

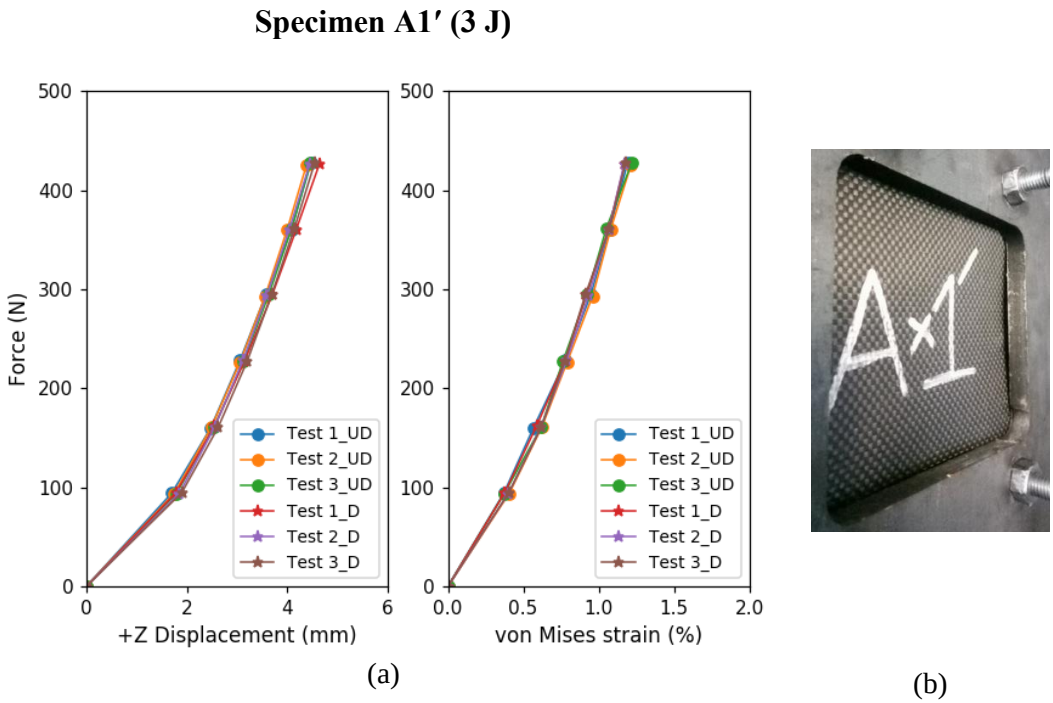

Figure 9: Full-field DIC results of specimen A1′ which was subjected to 3 J of impact energy: shows the force vs out-of-plane displacement curves and force vs von Mises strain curves, where "UD" stands for undamaged and "D" stands for damaged, (b) shows the specimen after the impact

Figure 10 and Figure 11 shows the full-field DIC results of specimens B3′ and A2. Specimen B3′ was subjected to a higher centered impact energy of 6 J and A2 was subjected to 9 J. The force vs out-of-plane displacement curves of B3′ in Figure 10(a) show no noticeable peak deflections of the specimen before and after the impact of 6 J. The force vs von Mises strain curves however in Figure 10(a) show a change in maximum strain of the specimen after the impact. The impact energy of 6 J caused enough damage that it could be detected using full-field DIC from strain data. The force vs von Mises strain curves show a more compliant specimen after the impact for all repeated tests. The von Mises strain values are in agreement for all tests well within the expected range of variance between tests (i.e. 0 - 2 % von Mises strain). The lack of distinction on the force vs out-of-plane displacement curves between the undamaged and damaged specimen may be due to the amount of flexibility of the specimen. The specimen reverted back to its original shape once it was unbolted.

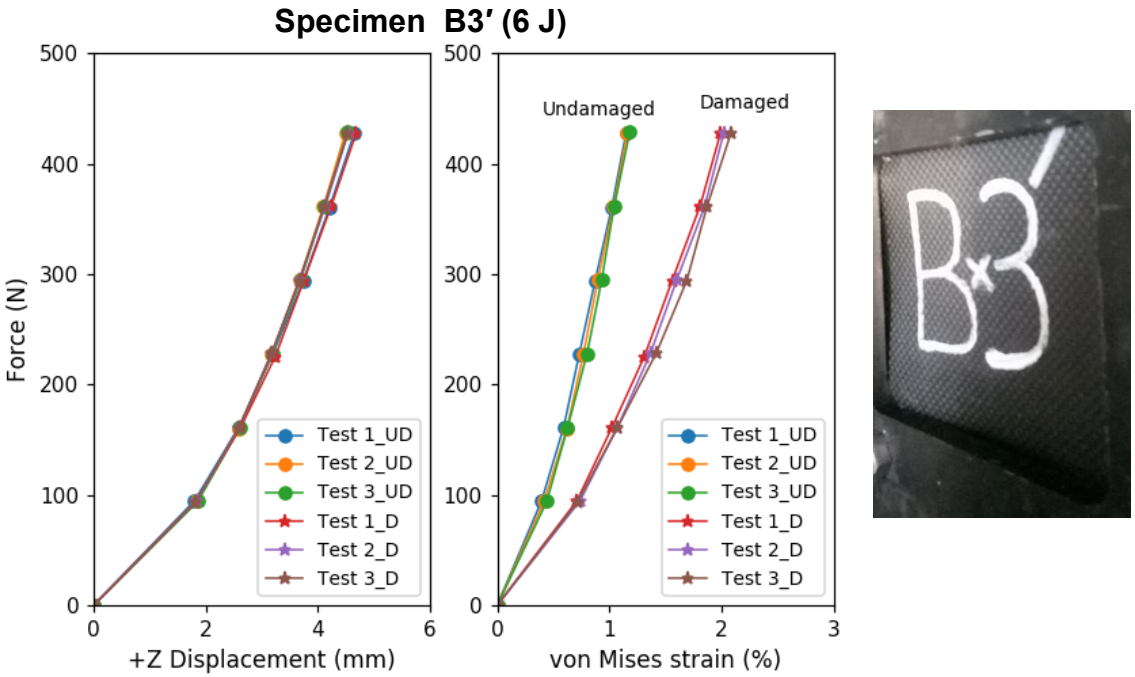

(a) (b)

Figure 10: Full-field DIC results of specimen B3′ which was subjected to 6 J of impact energy: (a) shows the force vs out-of-plane displacement curves and force vs von Mises strain curves, where "UD" stands for undamaged and "D" stands for damaged, (b) shows specimen B3′ directly after impact

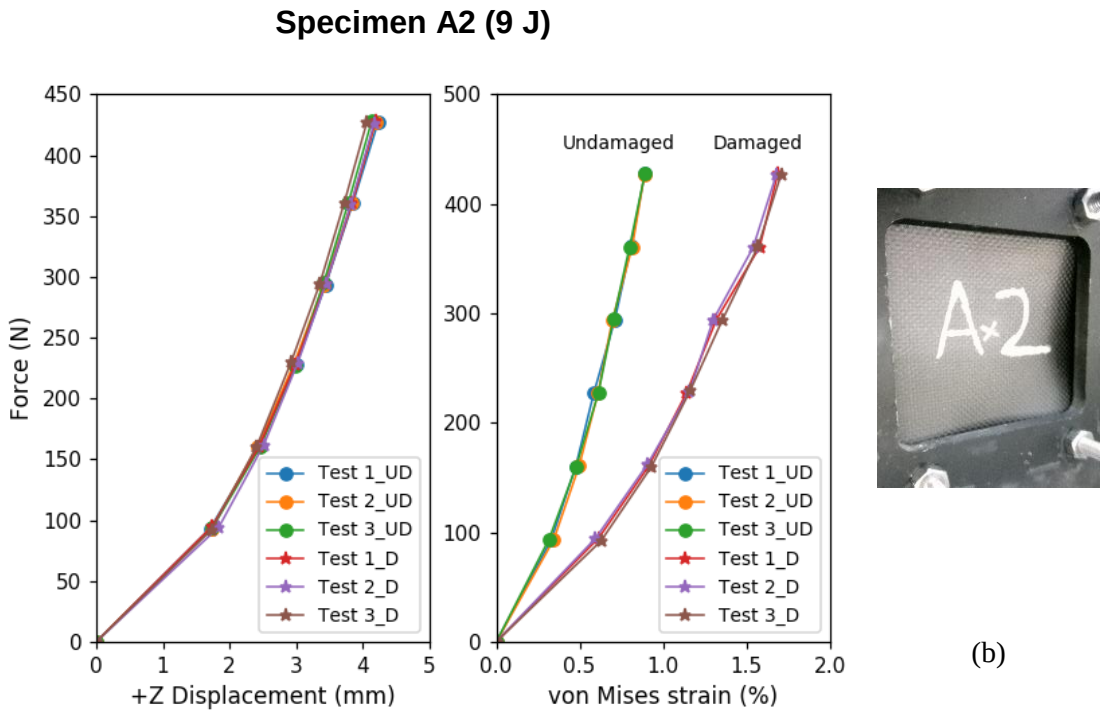

(a) (b)

Figure 11: Full-field DIC results of specimen A2 which was subjected to 9 J of impact energy: (a) shows the force vs out-of-plane displacement curves and force vs von Mises strain curves, where "UD" stands for undamaged and "D" stands for damaged, (b) shows specimen A2 directly after impact

Figure 11(a) shows the force vs displacement curves and force vs von Mises strain curves of specimen A2 which was subjected to 9 J of centered impact energy. No noticeable difference exists on the force vs displacement curves between the undamaged and damaged A2 specimen. The reduction in stiffness due to the damage caused by the impact is evident on force vs von Mises curves, the difference in von Mises values increased with increasing load with no significant variation between repeated tests. Figure 11(b) shows the deformation of specimen A2 immediately after the impact, the specimen reverted back to its original shape once removed from the base plate due to its flexibility.

5.3 Full-field DIC results of specimens subjected to off-center impact energies

Figure 12 shows the force vs displacement curves and force vs von Mises strain curves of the specimen A3 that was subjected to off-center impact of 12 J.

The results show that apart from the established variation between tests there is no noticeable reduction in stiffness on the force vs displacement curves and on the force vs von Mises strain curves of specimen A3. Similar results were obtained for the specimens that were subjected to 3 J, 6 J, and 9 J of impact energies. The off- center impact locations were marked at different points on all the specimens and the loading was always applied at the center of the specimens during full-field DIC. From the curves of specimen A3 which received the highest impact energy, it is clear that full-field DIC cannot detect barely visible impact damage when the load is not applied near the damage area.

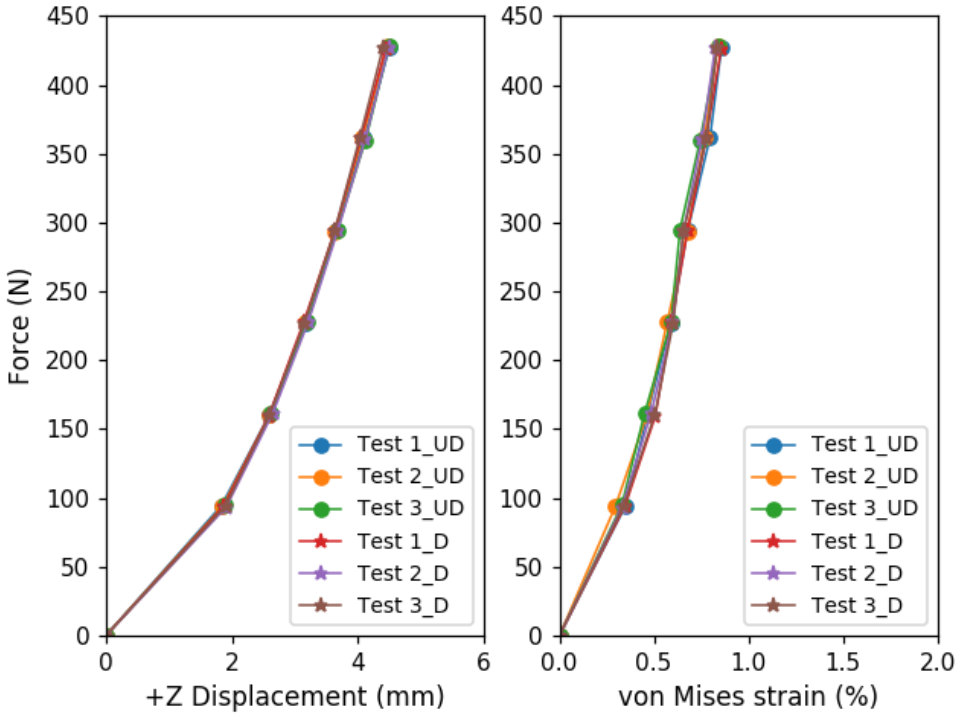

Figure 12: Full-field DIC results of specimen A3 that was subjected to off-center impact energy of 12 J. Where “UD” stands for undamaged and “D” stands for damaged

Figure 13 shows a plot of the change in von Mises strain vs impact energy of all the specimens that were subjected to centered and off-centered impact damage. The plot shows that the change in von Mises strain for the specimen that was subjected to 6 J of centered impact (B3′) exceeds that of the specimens that were subjected to 9 J (A2) and 12 J (B2) centered impact energies by 0.1 % and 0.08 % respectively. This can be attributed to the variation that exists in full-field DIC measurements.

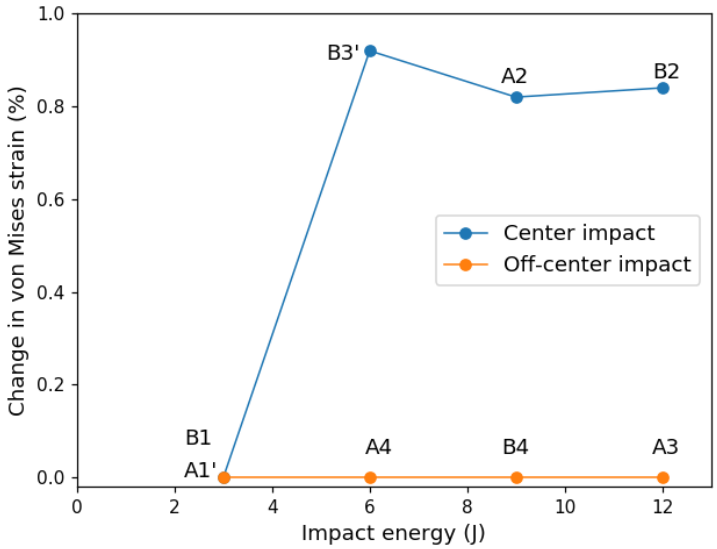

Figure 13: A plot of the change in von Mises strain vs impact energy of all specimens subjected to centered and off-centered impact energies

6. CONCLUSIONS

The work presented in this paper focused on using full-field DIC under static loading conditions as a technique for detecting barely visible impact damage in laminated composites induced by varying centered and off-centered impact energies. The subject of the experiments were 156 mm × 133 mm × 1mm carbon/woven laminated composites. As a result of their flexibility, no noticeable change in stiffness exists on the force vs out-of-plane displacement curves of all the specimens subjected to varying centered and off-center impact energies.

The results show that the loss in stiffness due to impact damage is more pronounced on the force vs von Mises strain curves of all the specimens subjected to centered impact energies. The results show that the difference in von Mises strain values between the undamaged and damaged specimen increases as the load increases. From the results full-field DIC is capable of detecting barely visible impact damage caused by energies equal or greater than 6J. For the specimens subjected to off-centered impact, no noticeable changes in stiffness exist between the undamaged and damaged specimens on both the force vs out-of-plane displacement curves and the force vs von Mises strain curves apart from the established variation between tests. The von Mises strain fields of specimen B2 which was subjected to 12 J of centered impact show that full-field DIC under static loading conditions can detect barely visible impact damage when the load is applied near the damaged area.

The application of full-field DIC as an NDT method presented in this paper is beneficial when the interest is in the change in stiffness of the material, additional parameters of the damage such as the damage size and depth cannot be obtained using this method. The variations in full-field DIC measurements make it difficult to correlate damage extent to impact energy, as shown in figure 13 the change in von Mises strain of the specimen that was subjected to 6 J of impact exceeds that which was subjected to 9 J. Small specimens were used in the experiments and the location of the damage was known. For larger specimens without any knowledge of the damage location, the presented method of using full-field DIC will not be fruitful especially when the loading does not excite enough of the damaged area. The other NDT methods discussed do not have this limitation and some can give damage parameters (ultrasonic C-scan). The work presented in this paper demonstrates that full-field DIC can be used to detect barely visible impact damage in laminated composites provided that the location of the damage is known and the loading is applied near the damaged area.

REFERENCES

[1] Jareteg, C., Wärmefjord, K., Cromvik, C.,Söderberg, R., Lindkvist, L.,Carlson, J., Larsson, S., Edelvik, F. (2014). Geometry Assurance Integrating Process Variation with Simulation of Spring-In for Composite Parts and Assemblies. *Journal of Computing and Information Science in Engineering*

[2] Matthews, F.L., Rawlings, R.D. (1999).*Composite materials: Engineering and science*. New York: CRC press

[3] Park, J.H., Hwang, J.H., Lee, C.S., Hwang, W. (2001). Stacking sequence design of composite laminates for maximum strength using genetic algorithms. *Composite Structures, Volume 52, Issue 2, 2001, Pages 217-231*

[4] Gholizadeh, S. (2016). A review of non-destructive testing methods of composite materials. *Procedia Structural Integrity* **1** (2016) 050–057

[5] Meyendorf, N.G.H., Nagy, P.B., Rokhlin, S. (2013). *Nondestructive Materials Characterization: With Applications to Aerospace Materials*: Springer Berlin Heidelberg

[6] Manes, A., Nunes, S., González-Jiménez, A., Amico, S., Giglio, M. (2018). Comparison of Non-Destructive Techniques for Impact Damage Area Assessment in Aramid/Epoxy Composites. *Proceedings* 2018, *2*, 437

[7] Garney, G. (2006). *Defects found through non-destructive testing methods of fiber reinforced polymeric composites*. California State University: Fullerton

[8] Kersemans, M., Verboven, E., Segers, J., Hedayatrasa, S., Van Paepegem, W. (2018). Non-Destructive Testing of Composites by Ultrasound, Local Defect Resonance and Thermography. *Proceedings* 2018, *2*, 554

[9] Kessler, S.S., Spearing, S.M., Atalla, M.J., Cesnik, C.E.S., Soutis, C. (2002). Damage detection in composite materials using frequency response methods. *Composites: Part B* **33** (2002) 87-9

[10] Banks, H.T., Emeric, P.R. (1998). Detection of non-symmetrical damage in smart plate-like structures. *NASA/CR-1998-206931*

[11] Chrysafi. A.P., Athanasopoulos, N., Siakavellas, N.J. (2017). Damage detection on composite materials with active thermography and digital image processing. *International Journal of Thermal Sciences* **116** (2017) 242-253

[12] Faria, A.W., Silve, R.A., Koroishi, E.H. (2017). Matrix Damage Detection in Laminated Composite Structures by Discrete and Continuous Wavelet Transforms Using Vibration Modes. *Journal of Aerospace Technology and Management. São José dos Campos, Vol.9, No 4, pp.431-441*

[13] Spiegel, M.D. (2014). *Damage detection in composite materials using lead zirconate titanate.* (Msc). University of Alabama

[14] Rauter, N., Lammering, R. (2015). Impact Damage Detection in Composite Structures Considering Nonlinear Lamb Wave Propagation. *Mechanics of Advanced Materials and Structures, 22:1-2, 44-51*

[15] Schenk, T. (2005).Introduction to photogrammetry. *Department of Civil and Environmental Engineering and Geodetic Science*

[16] Won Nam, K., Park, j., Kim, I-Y., Kim, k-G. (2012). Application of Stereo-Imaging Technology to Medical Field. *Healthcare Informatics Research* **18** (2012):158-163

[17] Dowling, N.E. (2013). Mechanical Behaviour of Materials.4th edition. New York: Pearson.

[18] Segreto, T., Teti, R., Lopresto, V. (2018). Non-Destructive Testing of Low-Velocity Impacted Composite Material Laminates through Ultrasonic Inspection Methods.

[19] Aramis. (2009). User Manual-Software.